Journal of Materials Chemistry C

ROYAL SOCIETY OF CHEMISTRY

PAPER

View Article Online
View Journal | View Issue

Cite this: J. Mater. Chem. C, 2025, 13, 23620

Bismuth-doped soda alumino germanate glass part I: examination of the role of Na/Al atomic ratio on the glass matrix and bismuth luminescence properties in the 300–900 nm spectral range

Leanne J. Henry, *[a] Michael L. Klopfer,[b] Joshua D. Reding[c] and Kathleen A. Richardson[d]

A significant shift in luminescence spectra of bismuth-containing glasses was investigated for a range of non-bridging oxygen (NBO) containing glasses following excitation between 248–375 nm. Emission behavior variation for glasses was evaluated as a function of alkali to aluminum ratio which is known to vary the concentration of NBO thereby imparting locally different environments for multivalent dopant Bi ions. We report that the structural variation imparted by NBO variation significantly impacted the emission features of both the undoped base glass matrix as well as glasses containing Bi where emission features could be directly ascribed to defects within glasses and the changing Bi valence states. A significant shift in the luminescence spectra (out to 900 nm) between NBO containing and deficient undoped and bismuth doped glasses to shorter wavelengths was seen to occur. This was attributed to the differing defects which form in the two classes of glass matrices as well as a tightening of the glass structure as the Na/Al ratio was decreased. Specifically, we show that an NBO containing environment leads to red shifted absorption edges along with stabilization and emission from Bi^{2+} (615 nm) and Bi^{0} (810 nm) while NBO deficient environments enable stabilization and emission from Bi^{2+} centered at 750–795 nm. A transition in the luminescence and excitation spectra was seen to occur with increasing bismuth concentration in two different matrices containing NBOs when excited with 248 and 325 nm, respectively. These results show promise in leveraging the host glass matrix to directly influence the luminescence properties of the dopant.

Received 11th July 2025,
Accepted 6th October 2025

DOI: 10.1039/d5tc02646f

rsc.li/materials-c

1. Introduction

Significant attention has been devoted to the discovery and fabrication of active laser media to open up new applications to include fiber optical communications. At this time, there is a dramatic need to increase the capacity of optical communications systems[1–3] outside of the spectral region of 1530–1610 nm amplified by erbium doped silica lasers. Such expansion is possible because of the development of low-water glass having a maximum transmission loss below the acceptable level of 0.5 dB km^{-1} (ref. 4 and 5) in the 1250–1700 nm spectral range. Because bismuth exhibits broadband luminescence arising from transitions of the valence electrons which are highly sensitive to the local glass' crystal field environment, Bi-doped optical fibers have demonstrated lasing and amplification across this region and therefore potentially could enable expansion of the optical fiber communication bandwidth.[6–11]

In optical materials, bismuth ions can exist in a number of multivalence oxidation states: Bi^{0}, Bi^{+}, Bi^{2+}, Bi^{3+} and Bi^{5+}, in addition to Bi clusters and metallic colloidal particles, $(Bi)_n$.[12] When glasses are prepared with Bi_2O_3 as a starting material, the fraction of Bi in each oxidation state is impacted by the host matrix glass type (oxide, non-oxide), network former (silicate, borate, phosphate or germanate), composition/optical basicity of the glass matrix,[13] network environment (bridging or non-bridging cations), melt atmosphere, thermal history associated with the melt/annealing processes[14,15] and concentration of bismuth.[14] While the bismuth ion predominantly exists in the

[a] Air Force Research Laboratory, Directed Energy Directorate, 3550 Aberdeen Avenue SE, Kirtland AFB, NM 87117, USA. E-mail: leanne.henry.1@us.af.mil
[b] Leidos Inc., 2109 Air Park Road SE, Albuquerque, NM 87106, USA
[c] United States Air Force Academy, 2354 Fairchild Dr., Colorado Springs, CO, 80840, USA
[d] University of Central Florida, The College of Optics and Photonics, Department of Materials Science and Engineering, 4304 Scorpius Street, Orlando, FL 32816, USA

+3 and +5 states in oxide materials, they can follow a reduction pathway[12] resulting in the co-existence of multiple valence states;

$$Bi^{3+} \rightarrow Bi^{2+} \rightarrow Bi^{+} \rightarrow Bi^{0}, Bi_2, Bi_2^{-}, Bi_3, \ldots \rightarrow (Bi)_n \quad (1)$$

as well as clusters of various multi-atom sizes. While multiple valence states do not usually occur in crystalline media that have characteristic coordination sites, glasses, depending on their network configuration, can have a range of local environments with varying local charges that can thereby host bismuth ion in different oxidation states. Sharonov[16] examined the fluorescence decay dynamics of 87 mol% GeO_2-12 mol% AlF_3-1 mol% Bi_2O_3 glass and showed there to be multiple classes of bismuth optical emission centers arising from variation in the local environment. Effects of the glass matrix and melt environment have been seen in the past[17,18] with chromium doped aluminate glass samples containing +3, +4, +5 and +6 species when melted under oxygen and +3 and +4 species when melted only in argon as an example. In addition to charge balance, the physical molar volume available to accommodate the large Bi ion, is defined by the glass network's mean coordinate number (MCN) which is dictated by the number of bridging and non-bridging species. Non-bridging oxygen (NBO) containing glasses, in the case of oxide glasses, have lower MCNs and therefore offer larger volumes suitable for accommodating the larger Bi species.

The study of the emission properties of the various bismuth oxidation states is best done in crystals where bismuth in a single oxidation state will reside in characteristic coordination sites within a crystal lattice. The emission properties of bismuth emission centers having valencies between 0 and +3 in crystals that have been previously reported are collated in Table 1. Aside from the properties of known bismuth oxidation states in crystals summarized in Table 1, in germanium-containing oxide glass, an emission centered at 790 nm having a full width at half maximum (FWHM) of 100 nm and a lifetime of 1.12 μs is speculated to be associated with Bi^{2+} as this peak dominates when melted in an oxidizing environment relative to an emission located at 1200 nm thought to be due to Bi^{+}.[34] Our work further validates the conclusion that the emission seen in the 750–800 nm range in germanate containing glasses is from Bi^{2+}.

Germanate glasses are a host of interest for the bismuth emitter as multicomponent germanate glass have excellent properties in the infrared (IR) region which include low phonon energy and high transparency.[35–37] In addition, germanate glasses are also prone to form structural defects making it easier to form complex emission centers.[38,39] Germanate glass typically has a tetrahedral quartz-like structure,[40] however, in Na-containing germanate glass, some of the oxygens are located further from germanium atoms due to the presence of NBOs created by the presence of Na^{+} ions.[41] It is thought that co-doping with Al^{3+} can be used to reduce the NBO concentration, and as an initiator and dispersant for bismuth active centers (BACs), it can modify the local charge environment thereby enhancing the luminescence.[37,42,43] In silicate glasses,[40] upon the addition of Al_2O_3, each aluminum ion will remove one non-bridging oxygen and the network will tighten with the disappearance of NBOs. The bonding of aluminum to NBOs in germanates, thereby reducing the number, is believed to be similar. Chen[44] discussed the changes in luminescence emission between 850 and 1625 nm (460 nm excitation) from $(90 - x)$ GeO_2–xAl_2O_3–10BaO·5Bi_2O_3 glass when the amount of aluminum varied between 0 and 20 mol%. We will expand upon this in the present study of bismuth doped soda alumino germanate glass.

Matrix defects reported previously in naturally occurring germanate glass include the germanium lone pair center (GLPC) which is a two-coordinated germanium ion (Ge^{2+}) with a pair of electrons,[45] the non-bridging oxygen hole center which is a singly coordinated oxygen bonded to a germanium atom with an unpaired electron[46,47] and the E' center which is a three-fold coordinated germanium atom with an unpaired electron.[48,49] Relative to a glassy germanate network upon excitation at room temperature with 5.1 eV (243 nm), emission from the GLPC was seen to occur at 413 nm with a FWHM of 86 nm and a lifetime of 62 μs.[45] The associated excitation spectrum contained two bands located at 248 and 330 nm (FWHM of 35 and 31.5 nm, respectively) with ratio of the height

Table 1 Properties of Bi^{0}, Bi^{+}, Bi^{2+} and Bi^{3+} in crystalline host matrix

Bi ion	Center wavelength range [nm]	FWHM range [nm]	Range of lifetimes [μs]	Excitation band peak ranges [nm]	Ref.
Bi^{3+}	290–480		0.045–0.41	Bi:Sc/Y/La:233 to 341 nm Bi:$CaSO_4$:243, 303, 354 nm Bi:$Ba_5SiO_4Cl_6$:230 to 340 nm	Bi:Sc/Y/La in a variety of crystals,[19] Bi:$CaSO_4$,[20] Bi:$Ba_5SiO_4Cl_6$,[21] Bi:$Lu_2Ga_5O_{12}$,[22] Bi:YOCl,[23] Bi:YBO_3,[23] Bi:$YAl_3B_4O_{12}$,[23] Bi:YPO_4[23]
Bi^{2+}	585–700	40–60	4–10.6	655 nm window ($Ba_2B_5O_9Cl$:Bi):273, 440, 624 nm 639 nm window ($BaBPO_5$): 260, 432, 622 nm 628 nm window ($CaBPO_5$): 250, 421, 584 nm	Bi:SrB_4O_7,[24] Bi:$BaSO_4$,[25]Bi:Sr/$BaSO_4$,[26] Bi:$Sr_2B_5O_9Cl$,[27]Bi:$BaBPO_5$,[28] Bi:$CaBPO_5$,[29] Bi:$Ba_2B_5O_9Cl$[29]
Bi^{+}	950–1560	125–250	140–2200	1240–1270 nm window: (1 : 1.054$CsGaGe_2O_6$: Bi): 523, 750 nm	Bi:$KAlCl_4$,[30] Bi:$RbPb_2Cl_5$,[31]Bi:CsI[32]
Bi^{0}	990–1280	129–231	17.2–46.4	990 nm window (Bi:$Sr_2B_5O_9Cl$): 322, 369, 460 625 nm 1055 nm window (Bi:$Ba_2B_5O_9Cl$): 298, 378, 478, 534 (sh), 665, 850nm 1280 nm window (Bi:$Sr_2B_5O_9Cl$): 292, 338, 428, 540 nm	Bi:$Sr_2B_5O_9Cl$,[27]Bi:$Ba_2B_5O_9Cl$[33]

of the peak centered at 330 nm to that centered at 248 nm of 3.124. The characteristics of a similar emission seen from soda alumino germanate glass having Na/Al = 2 upon excitation with 248 nm will be compared. A broadband emission is also seen from a germanate containing matrix and is attributed to the presence of NBOs.[50,51] An example of this is the broadband luminescence centered at 590 nm (FWHM ~ 200 nm)[51] upon excitation of the glass: $3CaO–1Ga_2O_3–3GeO_2$ between 275 and 350 nm. This was attributed to the breakage of a O–Ge bond leaving a non-bridging oxygen hole center (NBOHC) and a germanium E' center. Luminescence here was attributed to the recombination of NBOHCs with germanium E' center as supported by electron spin resonance (ESR) data.[51] The properties of a similar emission from soda alumino germanate glass for Na = ∞ and 2 for excitations of 248, 325 and 375 nm will be discussed.

The 300–900 nm spectral range was chosen for study as the matrix emits in this region when excited in the UV. To summarize, the formation and stabilization of BACs responsible for visible and near infrared bismuth related emission is dependent on the host glass network and defects. The primary focus of the work in this paper is directed at investigating the effect of the Na/Al ratio in a bismuth doped germanate matrix on the emission properties of the bismuth and matrix. Following an examination of the impact of the NBO content on the properties of the base glass matrix, an evaluation of the Bi valence states stabilized along with their emission properties in these environments is presented. For the first time, a correlation between the matrix environment and bismuth emission in the 300–900 nm spectral range is presented for soda alumino germanate glass as well as how both the matrix and bismuth emission evolve with concentration of bismuth when the matrix contains NBOs. Finally, a future publication will study bismuth emission in the 900 to 1600 nm spectral range where matrix emission is generally absent when excited at longer wavelengths.

2. Experimental

2.1. Sample preparation

The preparation of sodium alumino germanate glass was dependent on the melt temperature, the length of time required to melt the raw materials as well as how the melt temperature/time would affect the reduction equilibrium of bismuth. In a hot glassy melt, the bismuth ions change oxidation state by interacting with components of the matrix resulting in both oxidation and reduction. As the melt progresses, an equilibrium is believed to be established relative to the distribution of bismuth oxidation states within the glass and when cast, the matrix will arrange itself to achieve electric neutrality throughout. Melting a material at too high of a temperature and/or in an atmosphere poor in oxygen and/or for too long of a period of time will reduce the bismuth to metal by driving oxygen out of the material *via*:

$$Bi^{(x+n)+} + \frac{n}{2}O^{2-} \rightarrow Bi^{x+} + \frac{n}{2}O_2 \quad (2)$$

This results in a glass having near zero transparency in the visible and near infrared. In addition, this is amplified as the concentration of Bi_2O_3 is increased. Thus, the proper selection of melt temperature and time is important if the optical properties of the glass in the visible/near infrared (NIR) are to be studied. Because of the dependencies of the bismuth reduction equilibrium on melt temperature/time, a glass containing a very low concentration of bismuth melted at a very high temperature could potentially contain more lower valence bismuth active centers (Bi^0 and Bi^+) thought to be responsible for near infrared emission[52,53] than a glass containing a higher concentration of bismuth melted at a lower temperature. The effect of melt temperature and time influenced the choice of bismuth concentration for the sodium excess and deficient glasses examined here.

Four types of glass matrices with varying ratios of Na/Al were investigated as shown in Table 2 below. The materials utilized were as follows: (1) Thermo Scientific – GeO_2, 99.999% (trace metals basis), (2) Sigma Aldrich – Al_2O_3, 99.99% (trace metals basis), (3) Alfa Aesar – Na_2CO_3, 99.997% (trace metals basis), and (4) Alfa Aesar – Bi_2O_3 – 99.999% (trace metals basis). The mol% of GeO_2 shown is that associated with the base glass composition. With the addition of bismuth, the mol% of GeO_2 is reduced by an amount equivalent to the mol% of Bi_2O_3.

Table 2 Composition of materials discussed in this paper, in mol%

	Mol% of component			
Component	NBO high	NBO low	NBO zero	NBO zero-
GeO_2	90*	85*	90*	92.5*
Al_2O_3	0	5	5	5
Na_2O	10	10	5	2.5
Bi_2O_3	0, 0.01, 1	0, 0.01, 1	0, 0.003	0, 0.003

The glasses were prepared by first thoroughly mixing the batched raw materials. The melting of aluminum containing materials in alumina crucibles and non-aluminum containing materials in platinum crucibles was carried out to avoid contamination. NBO high/NBO low glasses were melted at 1350 °C for 3 hours while the higher melting NBO zero/NBO zero- glasses were melted at 1625 °C for 20 and 25 minutes for the case of doped and undoped materials, respectively. Once melted, the glass was cast into a steel mold at room temperature. Annealing was not carried out as the cast glass was stable in addition to being more representative of the glass in an optical fiber after draw. In addition, annealing has also been shown to alter the luminescence properties of the material.[54] The following characteristic properties of the samples are shown in Table 3 below: thickness, density, characteristic temperatures and the index of refraction at 632 nm. Of note is that $T_x–T_g$ is greater than 100 °C for all of the material types.

The decision to melt NBO high/low glasses at a lower temperature than 1625 °C was made after it was determined to not be feasible to prepare the NBO high/low glass matrices under the same conditions as the higher melting NBO zero/zero- glasses. When 0.003 mol% Bi_2O_3 doped NBO high/low

Table 3 Characteristic properties of undoped NBO high/low/zero/zero- glasses

Glass	Thickness [mm]	Density [g cm^{-3}]	T_g [°C]	T_x [°C]	T_x–T_g [°C]	Index of refraction
NBO high	12.43	4.017	516.3	644.6	128.3	1.63 ± 0.06
NBO low	11.99	3.630	509.7	725.3	215.6	1.63 ± 0.07
NBO zero	11.8	3.546	557.0	844.8	191.7	1.62 ± 0.05
NBO zero-	11.11	3.578	578.2	751.3	173.1	1.64 ± 0.06

glass matrices were melted at 1625 °C for 20–25 minutes in alumina crucibles, *i.e.*, platinum crucibles could not be used because of the melt temperature and the luminescence spectra of these glasses resembled those associated with the sodium deficient NBO zero/zero-glasses; see Section S1 of the SI and Fig. S1 for more detail. The conclusion drawn was that aluminum likely leached from the crucibles making the resulting glasses NBO deficient. This is not surprising since, previously, aluminum has been found in non-aluminum containing glasses when melted in alumina crucibles.[42] Since the objective here was to prepare both sodium excess and deficient series of glasses, a melt temperature of 1350 °C was utilized for the sodium excess materials.

2.2. Sample characterization

Density, differential scanning calorimetry and index of refraction measurements were carried out on the undoped NBO high/low/zero/zero- glasses. The density was measured with an AND GX-1000 five times using Archimedes method and then averaged. Differential scanning calorimetry was performed using a Netzsch STA449 Jupiter F3 by heating the NBO high/low glasses to 1100 °C and the NBO zero/zero- glasses to 1300 °C, both at 10 °C/min. Three runs on each sample were performed with the resultant T_g and T_x averaged. Finally, the refractive indices were measured by tracing the path of a red Melles Griot HeNe, 632 nm laser through a sample with application of Snell's law. Twelve separate measurements were made on each sample with the results averaged.

Absorption measurements in the ultraviolet (UV) to NIR were performed on a PerkinElmer Lambda 950 UV-Vis-IR absorption spectrometer using an integrating sphere. Absorption and transmission spectra were measured from 250–2000 nm in 2 nm steps on as-cast specimens nominally 11 mm thick. No additional polishing was done on the samples.

Luminescence and excitation spectra were measured on an Edinburgh Instruments FLS 1000 using a 450 W xenon lamp having a spectral range of 230–1000 nm along with detectors suitable for the range of emission. Fluorescence lifetimes were measured on the same instrument using a xenon flashlamp having pulse widths between 1.5–2.5 μs, average power up to 60W and a repetition rate of 0.1–100 Hz along with a 15 nm emission window.

Energy dispersive spectroscopy (EDS) was performed on a Tescan Vega3 XMU scanning electron microscope. The instrument was equipped with a LaB_6 electron gun for high-resolution imaging or tungsten filament for high current applications, with analysis over suitably large areas to allow quantitative sampling.

Additional details of the measurements of luminescence spectra, excitation spectra, fluorescence lifetimes and energy dispersive spectra can be found in Section S2 of the SI.

3. Results and discussion

For both undoped and bismuth doped NBO high/low/zero/zero-matrices (as defined in Table 2), spectroscopic analysis was carried out. The absorbance spectra were obtained with the resulting variation discussed below. Next, upon variation of the composition/NBO status of the matrices, the emission characteristics arising from the undoped matrix as well as with the bismuth dopant will be discussed for excitation wavelengths of 248, 325 and 375 nm. In addition, the characterization of specific emissions from both the matrix and bismuth were assessed and compared to prior studies. Lastly, the interaction of bismuth with the matrix *via* variation of the concentration of bismuth was evaluated, first, for the NBO low matrix excited with 248 nm and, second, for the NBO high matrix excited with 325 nm. These findings are discussed below.

3.1. Impact of the glass matrix and bismuth dopant level on the absorbance spectra

The absorbance spectra associated with undoped and 0.01/1 mol% Bi_2O_3 doped NBO high/low glasses, undoped and 0.003 mol% Bi_2O_3 doped NBO zero/zero- glasses are shown in Fig. 1a, b, c, and d respectively. (Note that the absorbance spectra were not corrected for Fresnel loss (sample thickness, $t \sim 11$–12 mm) for the different glass types.) As can be seen, the undoped host matrix absorption band edges for all compositions range from 352 (3.52 eV) to 313 (3.96 eV) nm for NBO high to zero- glasses, respectively, with glasses having the highest NBO concentration having the lowest energy (red shifted) UV edge. The corresponding Gaussian fits to the curves are shown as insets on each plot in Fig. 1 as well as in full size in Section S3a of the SI, Fig. S2. Absorbances centered in the ~435–550 (2.85 to 2.25 eV) nm and/or ~635–885 (1.95 to 1.40 eV) nm spectral ranges associated with lower valence bismuth and NIR emission[52,53,55] were seen in Fig. 1a–d. Even at the low doping concentration of 0.003 mol% Bi_2O_3 in the NBO zero/zero-matrices, the strengths of the absorbances centered at ~435–550 (2.85 to 2.25 eV) nm and ~635–775 (1.95 to 1.60 eV) nm, Fig. 1c and d, suggest there is a substantial quantity of bismuth in the lower oxidation states. It also should be noted that even though only 0.003 mol% Bi_2O_3 was doped into the NBO zero/zero- glass matrices, the amplitudes of the absorption bands centered around ~435–550 nm and ~635–775 nm in these glasses were 1.52–4.56 and 2.83–3.76 times stronger, respectively, than those associated with 0.01 mol% Bi_2O_3 doped NBO high/low samples. This is the result of the higher melt temperature of 1625 °C associated with the NBO zero/zero- matrices pushing the reduction equilibrium toward lower valence bismuth, metal and clusters in these glasses by driving oxygen out of the matrix. A similar change in the shape of the absorption bands was seen for barium alumino germanate glass

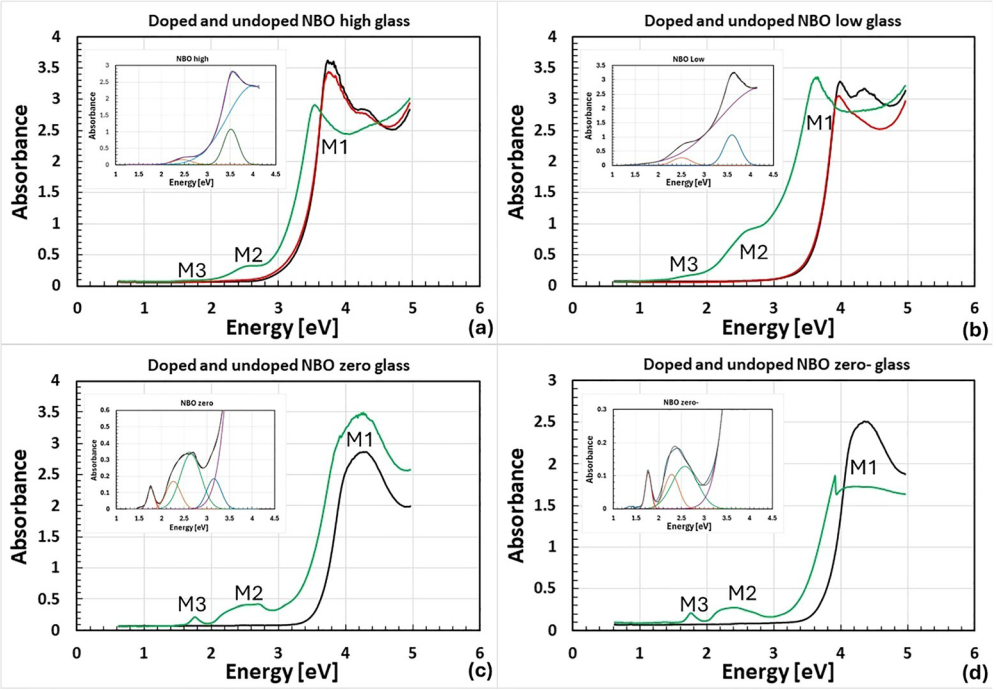

Fig. 1 Absorbance spectra *vs.* energy of undoped (black), 0.01 mol% Bi_2O_3 doped (red) and 1 mol% Bi_2O_3 doped (green) (a) NBO high and (b) NBO low glasses. Absorbance spectra vs energy of undoped (black) and 0.003 mol% Bi_2O_3 doped (green) (c) NBO zero and (d) NBO zero-glasses. Absorption manifolds 1, 2 and 3 are indicated by M1, M2 and M3, respectively. The absorbance spectra were not corrected for Fresnel loss (sample thickness, $t \sim 11$–12 mm) for the different glass types. Gaussian fits of absorbance spectra in energy space are shown as insets within the plots.

containing more Al than Ba relative to glasses containing less Al than Ba[44] with the authors attributing the strong peaks in the Al rich relative to Ba glasses to a greater number of bismuth active centers.

The absorbance spectra of the bismuth doped samples were fit with Gaussians as shown in the insets of Fig. 1a–d and Fig. S2, to aid in the discussion of the differences between bismuth doped NBO high/low and NBO zero/zero-glasses. The parameters associated with the fits are shown in Section S3b of the SI, Table S1a–d. Three distinct absorption manifolds are present in these materials, M1 to M3, as discerned by the fits of the absorbance spectra. Two separate Gaussians, one 2–3 times stronger in intensity than the other, drive the asymmetry seen in M2 (2.25 to 2.85 eV) of the absorbance spectra associated with NBO zero/zero- glasses. One can conclude that there are some differences in the energy levels associated with absorption in bismuth doped NBO high/low/zero/zero-glasses because of differing center wavelengths of the Gaussian fit peaks amongst the glasses. Further interpretation of the fits of the absorption bands can be found in Section S3 of the SI.

To conclude this section, three absorption manifolds were discerned *via* Gaussian fits. In addition, the absorptions associated with 0.003 mol% Bi_2O_3 doped NBO zero/zero- matrices melted at 1625 °C for 20 min around 435–550 and 635–775 nm were found to be 1.52–4.56 and 2.83–3.76 times stronger, respectively, than those associated with 0.01 mol% Bi_2O_3 doped NBO high/low glasses melted at 1350 °C for 3 hours because of oxygen being driven out of the matrix by the higher melt temperature resulting in bismuth being driven to metal and clusters. Next, the impact of the glass matrix type (NBO high/low/zero/zero-) on the luminescence emission of the undoped matrix as well as the bismuth dopant will be discussed in order to determine the impact of the presence of NBOs and a changed glass structure on the emission properties of bismuth.

3.2. Impact of the glass matrix and the bismuth dopant level on luminescence between 300 and 900 nm

We hypothesize that the formation and stabilization of bismuth active centers (BACs) responsible for visible and near infrared bismuth-related emission is likely dependent on defects in the glass matrix which in turn, are dependent on the concentration of NBOs that are dictated by the ratio of Na/Al associated with the matrix. For germanate glasses containing aluminum and sodium, the number of defect sites related to non-bridging oxygen is expected to decrease with the addition of aluminum, thereby reducing the number of negative charged sites available to modify the valence of a proximately located, charged bismuth ion. The aluminum will bond with the NBOs to form $[AlO_4]^-$ units which will be part of the matrix. The luminescence properties of the four types of glass matrices having varying ratios of Na/Al in the matrix were investigated in the 300–900 nm spectral range when excited at 248, 325 and 375 nm. Shown below in Fig. 2a–l are the luminescence spectra of both undoped and Bi_2O_3 doped NBO high/low/zero/zero-glass matrices. The collection parameters associated with these spectra varied across the series of samples (dwell time of 1 to 6 seconds, detector bandwidth of 2 to 15 nm and source slit of 0.5 to 8 nm) because of differences in strength of emission and

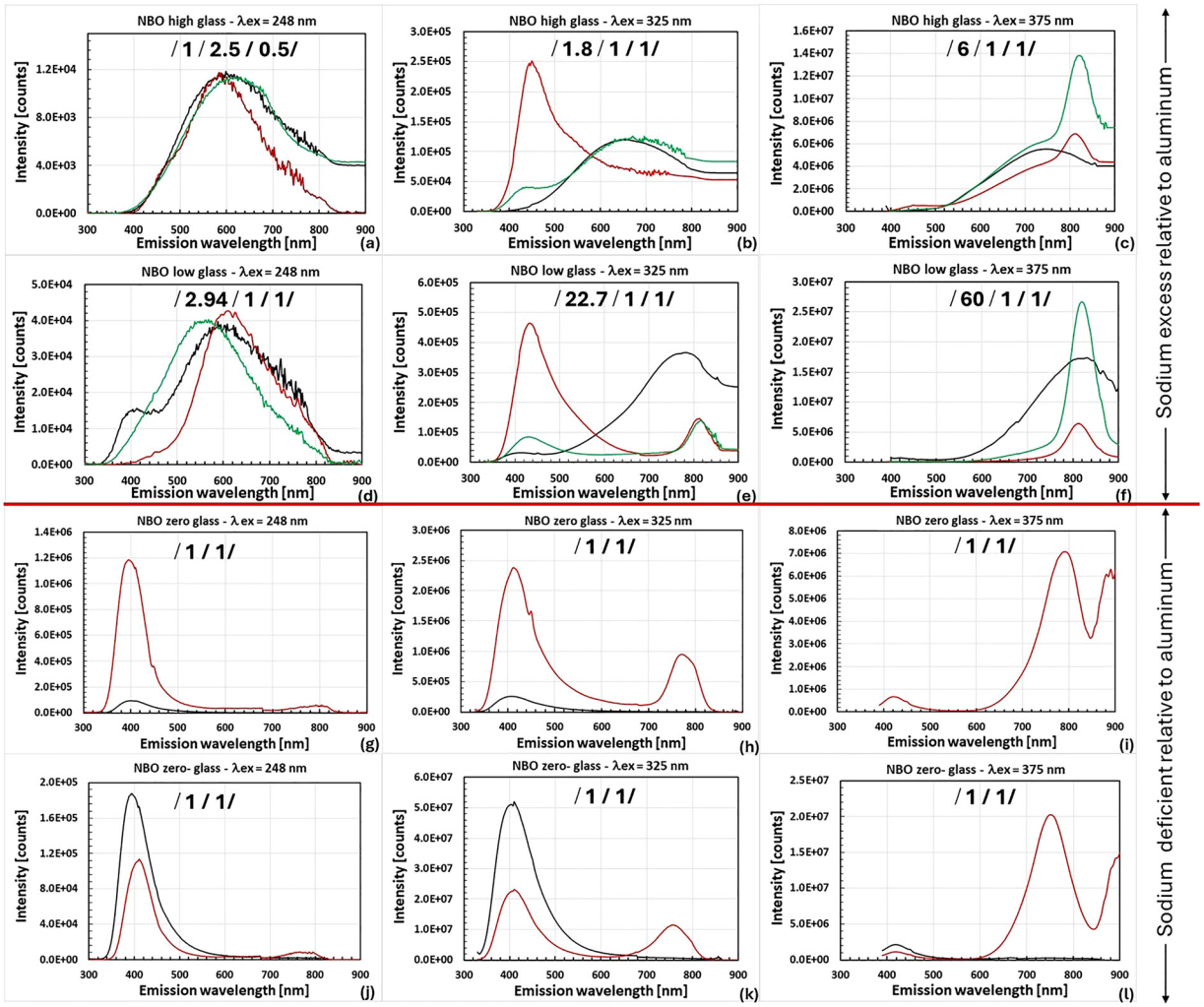

Fig. 2 Luminescence spectra between 300 nm and 900 nm for undoped (black) as well as 0.01 (green) and 1 mol% Bi_2O_3 doped (red) NBO high and NBO low matrices excited with (a) and (d) 248 nm, (b) and (e) 325 nm, and (c) and (f) 375 nm light. Luminescence spectra between 300 and 900 nm for undoped (black) as well as 0.003 mol% Bi_2O_3 (red) doped NBO zero and NBO zero- matrices excited with (g) and (j) 248 nm, (h) and (k) 325 nm, and (i) and (l) 375 nm light. The luminescence spectra in (a)–(f) and (g)–(l) are scaled by the values shown in the top center of each plot for the/undoped/0.01 mol% Bi_2O_3 doped glass/1 mol% Bi_2O_3 doped glass/samples and the/undoped glass/0.003 mol% Bi_2O_3 doped glass/samples, respectively.

the presence of an artifact in the ~410 nm spectral region associated with some samples. The relative strength of each peak shown next to the sample descriptions in the legend was determined by factoring in the collection parameters used assuming linear scalability as well as any arbitrary scaling factors applied to enable discernment of the peaks.

As can be seen in Fig. 2a–l, the emission properties of both the undoped and bismuth Bi_2O_3 doped matrices were found to vary depending on the sodium/aluminum ratio as well as the excitation wavelength. An apparent shift in the luminescence spectra between the NBO high/low and the NBO zero/zero- glasses for the three excitation wavelengths to shorter wavelengths is evident. This shift likely occurred because of the tightness of the matrix in the NBO zero/zero- glasses as a result of the lack of NBOs. This resulted in the crystal field at the location of the bismuth emitter in NBO zero/zero- matrices to be higher with similar emissions being shifted to shorter wavelengths and/or the emergence of emissions of a different origin. The wavelength of maximum emission shifts following 440 → 435 → 420 → 415 nm for the high energy emission envelope and 815 → 815 → 795 → 750 nm for the low emission envelope for NBO high/low/zero/zero- glass respectively. Previously, Chen[44] reported a shift in emission from $(90 - x)GeO_2$–xAl_2O_3–$10BaO{\cdot}5Bi_2O_3$ (x = 0–20) for glasses having Ba/Al > 1 relative to glasses having Ba/Al ≤ 1 for longer wavelength emissions between 850 and 1625 nm for excitation at 460 nm.

The general trends associated with luminescence emission of both undoped and bismuth doped NBO high/low/zero/zero- matrices were discussed for excitation at 248, 325 and 375 nm. Next, more specifically, luminescence from both undoped and bismuth doped NBO high/low matrices will be discussed in order to determine the effect of the presence (or absence) of aluminum on both the matrix and bismuth emission sites stabilized and their properties.

3.2.1. Emission behavior from the NBO high and NBO low matrices. The role of NBOs has been compared in two glass compositions to elucidate the role of high and low NBO concentrations on the resulting emission behavior in the 300–900 nm spectral range when excited between 248–375 nm. This region was examined because the matrix when excited with UV wavelengths displays emission. It needs to be noted that bismuth is usually known for emission in the 1000–1600 nm spectral range (see Section S5 of the SI, Fig. S3a–d for emission from NBO high/low/zero/zero- glasses when excited between 350–500 nm in the 700–1600 nm spectral range). Emission from bismuth in the NBO high/low/zero/zero- matrices in the 900–1600 nm spectral range when excited between 350–800 nm will be the subject of a future publication. The broadband matrix related emission from undoped NBO high/low glasses between 300 and 900 nm when excited with 248–375 nm, shown in Fig. 2a–f, is similar to the emission reported previously from alkali and alkaline earth containing germanates[50,51] involving the recombination of non-bridging oxygen with Ge E' centers. Also, the lifetime of the undoped matrix emission for a window of width 15 nm centered around the peak of the broadband emission tends to be multicomponent, see Section S3 of the SI, Table S2, which is indicative of multiple contributions to the emission. As an example, for undoped NBO low glass excited with 248 nm, the components of the lifetime of the broadband emission for a window centered at 580 nm are: 19.5 ± 0.1 μs (65.37%), 115 ± 3 μs (18.34%) and 550 ± 10 μs (16.29%). (Note that the percentages indicate the percent of the emission in each lifetime component.) Also, the shift in the center wavelength of the broadband emission as the excitation wavelength was increased is likely from a decreasing excitation of the resultant products. Shown in Fig. 3a is the luminescence spectrum for undoped NBO low glass excited with 248 nm along with deconvolution *via* Gaussian fits. It is conceivable that a component of the broadband emission centered at approximately 600 nm from the NBO high glasses melted in platinum crucibles could be from platinum contamination. This would be seen as a component of the envelop centered at approximately 680 nm as was previously reported from glasses of composition $1.0Na_2O$–$3.0SiO_2$ melted in air at 1400 °C in platinum crucibles.[56] One can see a slight asymmetry in this region in Fig. 2a which could be emission from platinum, however, it is much weaker than that of the main emission peak centered at ~600 nm. It should also be noted that the primary emission centered at roughly 600 nm was also seen in the NBO low glass which was not melted in platinum, but alumina. Therefore, we assess that if platinum emission is contributing to the luminescence, its effect is minor in comparison to the remainder of the emission profile.

The matrix related emission, Fig. 2d and 3a, centered at 414 nm with FWHM of 110 nm upon excitation with 248 nm in the NBO low glass has a primary lifetime component of 86 μs and is speculated to be attributed to the GLPC because of its resemblance to the emission previously observed in glassy germanate by Skuja[45] (λ_{ex} = 243 nm, λ_c = 413 nm, FWHM = 108 nm, τ = 62 μs). Shown in Fig. 5a is the excitation spectra associated with this emission for a window centered at 415 nm for the undoped NBO low glass. The excitation bands are centered at 262 nm (FWHM = 32 nm) and 344 nm (FWHM = 34 nm) with a ratio of the height of the peak centered at 344 nm to that centered at 262 nm of 1.258. The location of the excitation bands resemble those reported for the germanium lone pair center in glassy germanate by Skuja[45] (excitation bands: λ_{c1} = 248 nm (FWHM = 35 nm) and λ_{c2} = 330 nm (FWHM = 31.5 nm), ratio of the heights = 3.124). The excitation bands associated with the NBO low glass are at slightly longer wavelengths than those seen in glassy germanate. This difference as well as the difference in the ratio of heights could be due to the presence of aluminum and a different glass structure and/or charge balance.

The emission in the range of 400–450 nm appears only weakly in the luminescence spectra of the undoped NBO low glass when excited at 325 nm but develops at the 1 mol% Bi_2O_3 doping level in both the NBO high/low glasses, see Fig. 2b and e. Thus, we suggest that it is related to the presence of bismuth. The ~12 μs lifetimes measured from the 1 mol% Bi_2O_3 doped material (Section S4 of the SI, Table S3) are likely related to emission from the undoped matrix which has a multicomponent lifetime in both materials, as shown in Table S2, *i.e.*, both glasses have a component in the 18 μs range. It is a well-known fact that Bi^{3+},[19–23,57] a known emitter in this region, has a nanosecond range lifetime which is not measurable with our equipment. Also, the peaks of the excitation bands associated with this

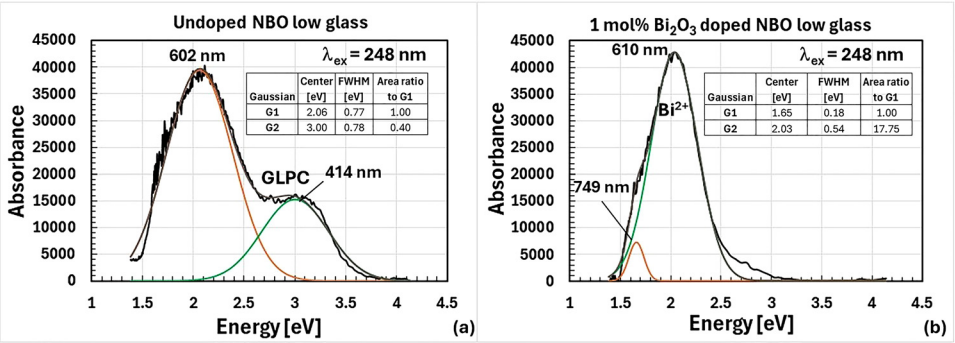

Fig. 3 Luminescence spectra (black) generated *via* excitation at 248 nm are shown for (a) undoped and (b) 1 mol% Bi_2O_3 doped NBO low glass along with the Gaussian fits in energy space (Gaussian #1 (G1) – orange, Gaussian #2 (G2) – green, Gaussian sum – brown) and the fit parameters (center energy [eV], FWHM [eV] and area ratio to G1).

emission in 1 mol% Bi_2O_3 doped NBO low (high) glass of 308 and 344 (354/348) nm, Fig. 4a and Section S6 of the SI, Fig. S4a, align best with those associated with Bi^{3+} in the crystal $CaSO_4$ (303 and 354 nm), see Table 1. This leads to speculation that the emission seen is from Bi^{3+} with weak emission from the matrix. Further work will need to be done to fully determine the identity of this emission. Additional information on the evolution of this emission with bismuth concentration from NBO high glass will be discussed in Section 3.3.2.

The bismuth related emission in both NBO high/low glasses when excited with 248 nm depicted in Fig. 2a and d, is likely due to Bi^{2+} because of the lifetime of 9.3 μs (Table S3) as well as the peak center location of 610–615 nm which is consistent with what has been previously observed for the emission of Bi^{2+} in crystals.[24–27] Also, the shortest wavelength excitation band peak centered at 272 nm, Fig. 4b, aligns with those seen from Bi^{2+} in $Ba_2B_5O_9Cl$ and BPO_5 of 273 and 260 nm, respectively, see Table 1. Simultaneous with the appearance of Bi^{2+} was the disappearance of the GLPC possibly *via* the following reaction:

$$Bi^{3+} + \text{-Ge-(GLPC)} \rightarrow Bi^{2+}\text{-Ge-(E' center)}. \quad (3)$$

It should also be noted that another contributing factor to the disappearance of the GLPC from the luminescence spectrum is likely absorption by bismuth which has strong absorption bands in this region. Also, the presence of aluminum in the NBO low matrix significantly strengthened this emission as evidenced by the dominant component of the emission lifetime of 9.3 μs increasing from 50% to 96.3% as shown in Table S3. The strengthening of this emission arose either from a bismuth emission configuration standpoint and/or the fact that the aluminum is enabling of a greater amount of Bi^{2+} since Al^{3+} cations in 4-fold coordination when replacing Ge^{4+} generate a localized negative charge, $[AlO_4]^{5-}$,[44] which can help stabilize Bi^{2+}. Shown in Fig. 3b is the Gaussian deconvolution of the luminescence emission from 1 mol% Bi_2O_3 doped NBO low glass excited at 248 nm. As shown in the figure, the broadband emission was fit with two Gaussians with the fit component centered at 610 nm (FWHM = 154 nm) speculated to be associated with Bi^{2+} emission while the longer wavelength component is speculated to be matrix emission that was not absorbed by bismuth which has weak absorption bands in this range.

The narrower bandwidth emission centered at 810–815 nm (FWHM of ~ 55–90 nm) for excitations of 325 (NBO low only) to 500 nm is absent from the luminescence spectra of the undoped NBO high and low glasses, Fig. 2b, c, e and f for excitations of 325 and 375 nm which display a broader bandwidth emission with FWHM of 240 nm. It is strongest when excited at longer wavelengths in the 400–500 nm (2.5 to 3.1 eV) spectral range, Section S5 of the SI, Fig. S3a and b because the amplitude of the excitation bands in this spectral region are 240–564 times stronger relative to that at 325 nm (3.8 eV) as shown in Fig. 4d and Fig. S4b. The presence of aluminum in the NBO low glass as well as increased concentration of bismuth is seen to generally enhance the formation of this emission. The lifetimes of the emission (16.8–31.4 μs in NBO high glass and 19.2–26.8 μs in NBO low glass at the 1 mol% Bi_2O_3 doping level), Table S3, are consistent with the lifetime of Bi^0 in crystals, Table 1. As bismuth in conjunction with silicon has been shown to emit in the 830 nm spectral range with a FWHM

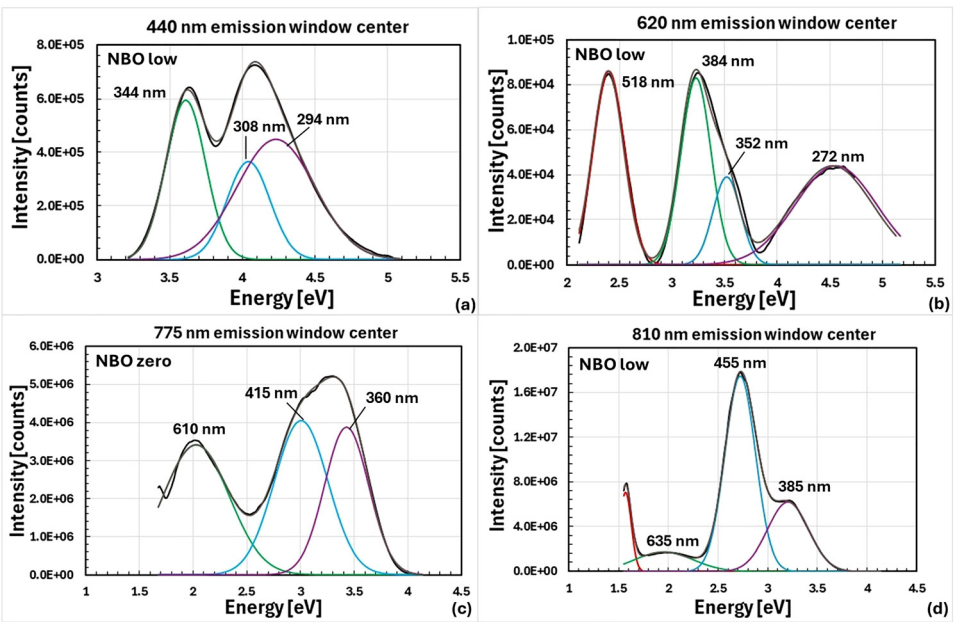

Fig. 4 Excitation spectra for emission windows associated with 1 mol% Bi_2O_3 doped NBO low glass centered at (a) 440, (b) 620 and (d) 810 nm. Excitation spectra for emission window associated with 0.003 mol% Bi_2O_3 doped NBO zero glass centered at (c) 775 nm. The peak center wavelengths of each of the Gaussian fit curves are shown in the plots. The plots include: raw data (black), sum of Gaussians (brown), individual Gaussians from longer to shorter wavelength (red, green, blue and purple).

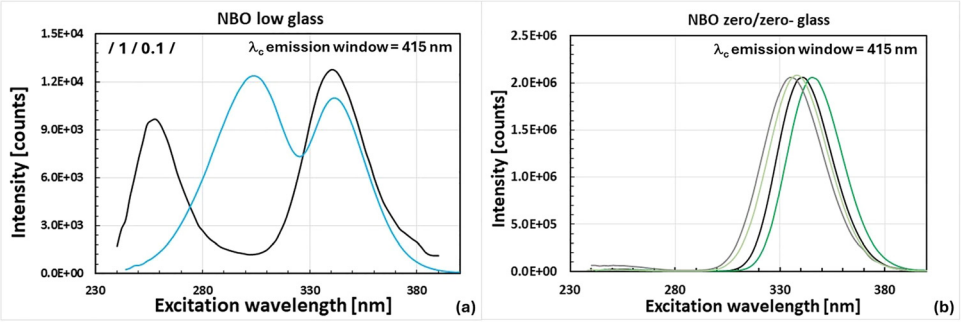

Fig. 5 Excitation bands associated with (a) NBO low glass (undoped (black) and 1 mol% Bi_2O_3 doped (blue)) and (b) NBO zero/zero- glasses (undoped (black/gray), 0.003 mol% Bi_2O_3 doped (green/light green)) for an emission window centered at 415 nm. Excitation spectra in (a) are scaled according to the numerical values in the top left corner for/undoped glass/1 mol% Bi_2O_3 doped glass/. Peaks of the spectra in Fig. 5b are normalized in the 350–370 nm spectral range.

of 24 nm and lifetime components of 0.301 and 6.8 μs,[58] Energy dispersive spectroscopy was performed to rule out contamination (at least above 0.1 at%) with silicon as the source of this emission. In addition, the glass was batched using high purity chemicals as described in the experimental section. This emission is thought to be related to Bi^0 even though it lies in a slightly shorter spectral range than emission of Bi^0 from crystals. The speculation concerning this is based on (1) the fluorescence lifetimes for excitation wavelengths of 325–500 nm which are consistent with the lifetime of Bi^0 (17–46 μs) in crystals[27,33] and (2) coincidence of the strongest two excitation spectra fit peaks with centers located at 394 (385) and 454 (455) nm in NBO high (low) glasses, Fig. 4d and S4b, with those associated with Bi^0 in $Ba_2B_5O_9Cl$ (1055 nm window) (378 and 478 nm)[33] and Bi^0 in $Sr_2B_5O_9Cl$ (990 nm window) (369 and 460 nm)[27] crystals, Table 1. The much smaller FWHM associated with this emission (~55–90 nm), Table S3, relative to the longer wavelength emissions centered between 1000–1400 nm (FWHM of 185–375 nm) is indicative of an emission environment of lower diversity that is possibly more compact.

Emissions from undoped and bismuth doped NBO high/low matrix excited with 248, 325 and 375 nm were discussed. It was observed that the undoped matrices emitted broadband light which shifted to longer center wavelengths as the excitation wavelength increased. The doped matrices supported: (a) emission possibly from Bi^{3+} centered at ~435–440 nm when excited with 325 nm, (b) emission thought to be from Bi^{2+} centered at ~610 nm when excited at 248 nm and finally (c) emission centered at ~810–825 nm thought to be from Bi^0 when excited with 325–500 nm. Next, emissions from both undoped and bismuth doped NBO zero/zero-matrices will be discussed in order to determine the impact of matrices deficient in NBO having a different structure on the valence state(s) of the bismuth stabilized as well as the excitation and emission properties of both the undoped matrix and the bismuth dopant.

3.2.2. Emission from the NBO zero and NBO zero-matrices. The emission seen from undoped NBO zero/zero-glasses located at a center wavelength of 400–425 nm (FWHM of 70–105 nm) as well as that seen in the doped analogs located in the range 410–425 nm (FWHM of 60–90 nm), both upon excitation with 248 and 325 nm, Fig. 2g, h, j and k, is an emission from the matrix in the undoped case and from the matrix plus possibly Bi^{3+} in the doped case. The primary lifetime component in the undoped material lies in the range 63–72 μs, Table S2, while in the doped glass, it lies in the range 37–81 μs, Table S3. Because of similarities with the known luminescence characteristics of the GLPC in glassy germanate,[45] the emission from the matrix could be from the germanium lone pair center. In these materials, as aluminum is less electronegative than germanium, it is possible that the charge balance could be such that more electrons would reside on the germanium atoms in the matrix thereby enabling lone pairs on a minority of atoms. For the case of both the doped and undoped NBO zero/zero-glasses, the excitation band centers were located in the range of 256 (FWHM of 24 nm) and 334–346 nm (FWHM of 28 nm) with the ratio of the intensity of the longer wavelength excitation band to that of the shorter wavelength excitation band of 24.5, Fig. 5b. The similarity of the location of the excitation bands to those of the GLPC in glassy germanate[45] also seems to indicate that this emission could be from the matrix. However, the peaks of the excitation bands for the doped samples in Fig. 5b also lie in the range of what has been seen from Bi^{3+} in crystals, Table 1, of 230–243 nm and 340–354 nm.[19–23] Hence, additional work is needed to enable identification of this emission.

The luminescence emission in the 750–795 nm wavelength range upon excitation with 325 to 450 nm, Fig. 2h, i, k and l and Section S5 of the SI, Fig. S3c, d, seen in bismuth doped glasses is not present in the undoped matrices and is related to bismuth. The emission is strongest when excited with 400 nm and the emission although 60 to 80 percent weaker, was also seen to occur when exited into the longer wavelength excitation band in the 550–700 nm spectra range. For excitation of 325–450 nm, this emission in bismuth doped NBO zero glass is centered in the region 755–795 nm (FWHM of 70–100 nm) with a primary component of the lifetime of 9.3–16.1 μs, Table S3. In bismuth doped NBO zero- glass, it is centered in the range 750–760 nm (FWHM of 70–100 nm) with a primary component of the lifetime of 9.52–14 μs, Table S3. The strongest peaks associated with fits to the excitation spectra, Fig. 4c

and S4c, are located at 360, 415 and 610 nm in Bi_2O_3 doped NBO zero glass. The first two peaks coalesce into one at 382 nm along with a peak at 622 nm in Bi_2O_3 doped NBO zero-glass. The excitation spectra for Bi^{2+} in $M^{2+}BPO_5$ (421–432 and 584–622 nm) (M = Ba and Ca),[28] Table 1, and $Ba_2B_5O_9Cl$:Bi (440 and 624 nm),[29] Table 1, tend to be in fairly good agreement with the peaks associated with the measured excitation spectra of NBO zero/zero- glass. Based on lifetime, similarity of the excitation peaks between Bi_2O_3 in NBO zero/zero- glass and Bi^{2+} in crystals in addition to spectral location although at a slightly longer wavelength than what has been observed from Bi^{2+} crystals, the speculation is that the emission in the 750–795 nm spectral range is from Bi^{2+}. Previously, researchers have seen an emission from bismuth doped germanate as well as alkali/alkaline earth gallium/aluminum germanate in the range 720–790 nm when excited with 280–360 nm light with a FWHM between 100–120 nm that they speculated could be attributed to Bi^{2+}.[14,34,59] Jiang's conclusion concerning the identity of this emission from 70 GeO_2–18 Li_2O–11 Ga_2O_3 when excited with 280–360 nm light was based on the dominance of this emission relative to the longer wavelength emission centered in the vicinity of 1150–1250 nm attributable to Bi^{+} when the melt was performed in an oxygen atmosphere.[34]

Luminescence emission from both undoped and bismuth doped NBO zero/zero- matrices was discussed. The possibility of the emission in the 400–425 nm spectral region in both undoped and doped glasses upon excitation with 248, 325 and 375 nm being due to the GLPC is discussed. The possibility of Bi^{3+} contributing to this emission in the doped glasses was also mentioned. Also, the emission in the 750–795 nm region found in doped matrices was speculated to be from Bi^{2+} based on position, lifetime and excitation peak information. Next, the evolution of emission as the concentration of bismuth is increased is discussed for NBO low matrices excited at 248 nm and NBO high matrices excited at 325 nm. This is being done to gain insight into the effect of bismuth doping concentration on the relative concentration of bismuth and matrix defects as discerned *via* luminescence and excitation spectra.

3.3. Evolution of emission from the matrix and bismuth with varying bismuth content

The role of Bi concentration on the attributes of emission was evaluated to gain insight into how the growth/diminishment of emission from both the matrix and bismuth emission centers were affected by the concentration of bismuth in the glass. It is expected that this would be related to the defect concentration in the glass matrix as well as the number of dopant ions residing in each valence state. We will first discuss the evolution of the luminescence and excitation spectra for 0 to 1 mol% bismuth doped NBO low glass when excited with 248 nm light. This was done to learn more about the rate of elimination of a matrix defect (possibly the GLPC) as the concentration of Bi^{2+} increased with bismuth doping concentration and whether there is a possible linkage between these processes.

3.3.1. Evolution of emission from the NBO low matrix upon addition of Bi_2O_3 when excited with 248 nm. An evolution in the spectral features of emission was found to occur for Bi_2O_3 doping concentrations between 0 and 1 mol% in NBO low glass. Shown in Fig. 6a–d are the luminescence spectra, excitation spectra for emission windows centered at 420 and 620 nm as well as the components of the lifetimes of emission for Bi_2O_3 doping concentrations between 0 and 1 mol%. The center wavelengths of the luminescence emissions, Fig. 6a and d,

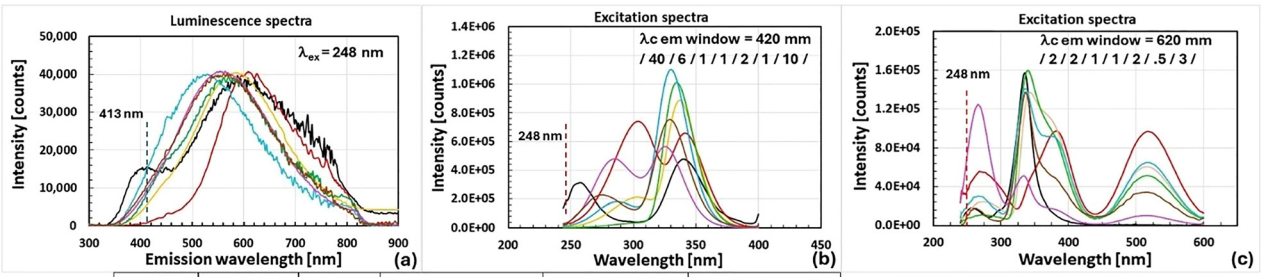

NBO low Mol% Bi_2O_3	Center wavelength [nm]	FWHM [nm]	Component #1 [μs]	Component #2 [μs]	Component #3 [μs]
0	585	298	19.5 ± .1 (65.37%)	115 ± 3 (18.34%)	550 ± 10 (16.29%)
0.01	550	276	17.1 ± .1 (55.67%)	102 ± 2 (23.07%)	540 ± 9 (21.26%)
0.05	568	224	16.0 ± .5 (25.81%)	112 ± 4 (35.04%)	630 ± 20 (39.15%)
0.1	550	226	3.22 ± .3 (52.52%)	14.6 ± .3 (39.77%)	240.0 ± 10 (7.71%)
0.5	588	212	7.7 ± .3 (88.13%)	35 ± 8 (9.47%)	240 ± 100 (2.40%)
0.75	582	222	11.08 ± .06 (96.96%)		210 ± 10 (1.41%)
1	615	140	9.3 ± .1 (96.31%)		160 ± 10 (3.69%)

(d)

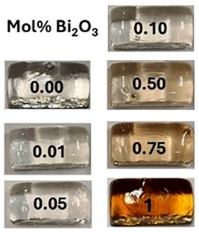

Fig. 6 (a) Luminescence for excitation with 248 nm as well as (b) and (c) excitation spectra for windows of width 15 nm centered at 420 nm and 620 nm, respectively, for 0 (black), 0.01 (brown), 0.05 (magenta), 0.1 (blue), 0.5 (green), 0.75 (yellow) and 1 (red) mol% Bi_2O_3 doped NBO low glasses. Curves in (a) are normalized at the peaks in the 500–650 nm spectral range. For curves (b) and (c), the luminescence peaks are scaled by factors in the top right hand corner for the spectra that correspond to/0/1/0.75/0.5/0.1/0.05/0.01/mol% Bi_2O_3 doping, respectively. (d) Components of the lifetimes of emission for excitation with a window centered at the peak of emission for each sample. The location of the peak of GLPC emission in glassy germanate at 413 nm is indicated by the blue dotted line in Fig. 6a.[45] The location of the excitation at 248 nm is shown in Fig. 6b and c by the red dotted line.

varied slightly, likely because of slight differences in the fabrication process conditions, however the FWHM of these curves is seen to decrease as the mol% Bi_2O_3 increased, Fig. 6d. The excitation spectra shown in Fig. 6b and c, underwent a complex evolution from the 0 to 1 mol% Bi_2O_3 doping level. The excitation bands (for windows centered at 420 and 620 nm) may have also evolved because of increasing incorporation of bismuth into the lattice. An evolution of the primary component of the lifetime of emission for a window centered at the peak of the broadband emission, Fig. 6d, toward that of Bi^{2+} is seen as the doping concentration of Bi^{2+} increased with the lifetime associated with Bi^{2+} starting to dominate that of the matrix at a Bi_2O_3 concentration of 0.5 mol%.

When bismuth reduced from Bi^{3+} to Bi^{2+}, the balance of charge within the doped matrix was affected resulting in a different distribution of matrix defects relative to the undoped glass because of fewer available electrons. Through this process, it is possible that the number of germanium lone pair centers were reduced or eliminated with formation of more electron deficient sites, *i.e.*, the Ge E' center. The emission feature speculated to be from the GLPC was not evident in the luminescence spectra at the 0.01 mol% Bi_2O_3 doping level, Fig. 6a. However, an evolution is evident in the excitation spectra, Fig. 6b, with the absorption in the 248 nm excitation region completely gone by a bismuth concentration of 0.50 mol% which is consistent with when the lifetime of Bi^{2+} begins to dominate that of the matrix.

The evolution of the emission centered in the 585–615 nm spectral region was discussed. As the concentration of bismuth was increased, emission associated with Bi^{2+} started to emerge at the 0.5 mol% doping level. Although the GLPC emission centered at ~400 nm was seen to disappear from the luminescence spectrum at the 0.01 mol% Bi_2O_3 doping level either from a change in the distribution of charge and/or bismuth absorption, absorption in the 248 nm spectral range for emission in a window centered at 420 remained also until the 0.5 mol% Bi_2O_3 doping level. Next to be discussed is the evolution of emission from both the NBO high matrix and bismuth emission centers for excitation at 325 nm when the concentration of bismuth was increased from 0 to 1 mol%. This is being done to understand the rate of growth of emission likely from Bi^{3+} centered at ~440 nm with the simultaneous diminishment of the broadband emission from the matrix centered at ~650 nm and whether these processes are linked.

3.3.2. Evolution of emission from the NBO high matrix upon addition of Bi_2O_3 when excited with 325 nm. Shown in Fig. 7a–e are the luminescence spectra, components of the lifetimes of emission and excitation spectra for emission windows centered at 450 nm, 620 nm and 810 nm, respectively, for 0 to 1 mol% Bi_2O_3 doped NBO high glass upon excitation with 325 nm. In Fig. 7a, the addition of Bi_2O_3 was seen to result in the diminishment of broadband emission from the matrix centered at ~650 nm along with the emergence of a strong emission centered at 440 nm which peaks at a Bi_2O_3 concentration level of 0.75 mol% Bi_2O_3. As the concentration of Bi_2O_3 was increased from 0 to 1 mol%, the lifetime associated with the matrix component of the emission centered at 450 nm evolved from being multicomponent to a single component

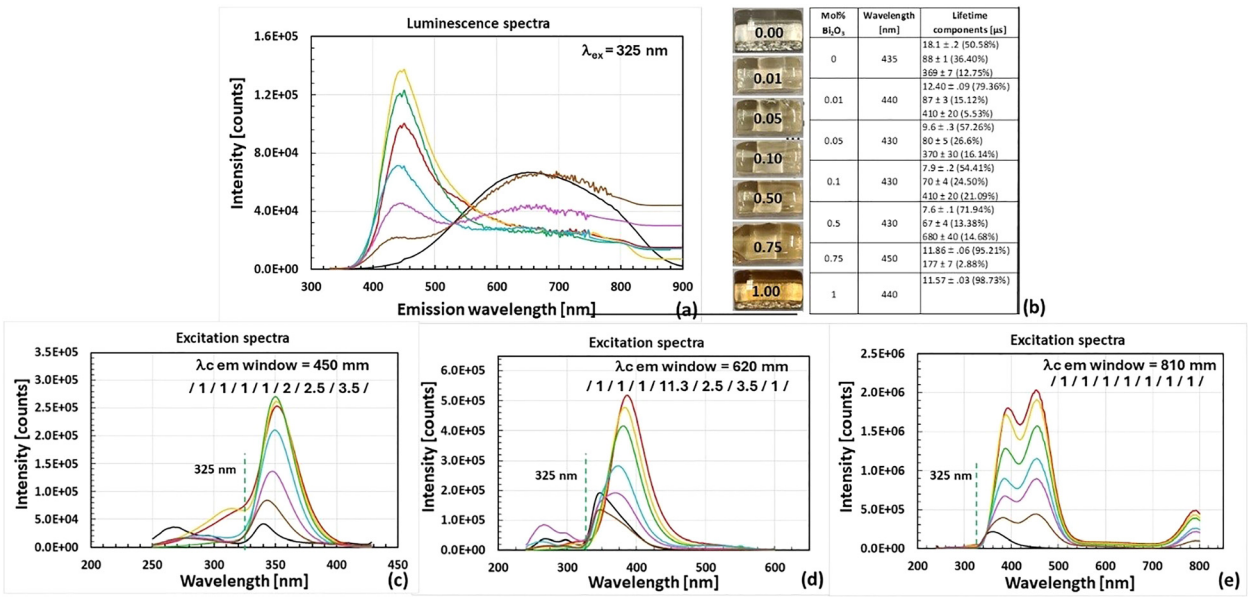

Mol% Bi_2O_3	Wavelength [nm]	Lifetime components [μs]
0	435	18.1 ± .2 (50.58%) 88 ± 1 (36.40%) 369 ± 7 (12.75%)
0.01	440	12.40 ± .09 (79.36%) 87 ± 3 (15.12%) 410 ± 20 (5.53%)
0.05	430	9.6 ± .3 (57.26%) 80 ± 5 (26.6%) 370 ± 30 (16.14%)
0.1	430	7.9 ± .2 (54.41%) 70 ± 4 (24.50%) 410 ± 20 (21.09%)
0.5	430	7.6 ± .1 (71.94%) 67 ± 4 (13.38%) 680 ± 40 (14.68%)
0.75	450	11.86 ± .06 (95.21%) 177 ± 7 (2.88%)
1	440	11.57 ± .03 (98.73%)

Fig. 7 (a) Luminescence for excitation of NBO high glass with 325 nm as well as (c), (d) and (e) the excitation spectra for windows of width 15 nm centered at 450 nm, 620 nm and 810 nm, respectively, for 0 (black), 0.01 (brown), 0.05 (magenta), 0.1 (blue), 0.5 (green), 0.75 (yellow) and 1 (red) mol% Bi_2O_3 doping. Note that the luminescence curves were normalized to align the minimum point in the 520–560 nm spectral range for samples having waning matrix emission in the 550–750 nm spectral range. For curves (c)–(e), the scaling factors of the excitation curves are indicated in the top of each plot for/0/1/0.75/0.5/0.1/0.05/0.01/mol% Bi_2O_3, doping. The location of the excitation at 325 nm is shown in (c) and (d) by the blue dotted line. (b) Components of the lifetimes of emission for excitation with a window centered at the peak of emission in the 430–440 nm spectral range for each sample.

with the primary component remaining in the range 7.6 to 18.1 μs, Fig. 7b. The associated excitation spectra, Fig. 7c, indicate that the influence of the matrix lasts in the 325 nm spectral range until approximately the 0.75 mol% Bi_2O_3 doping level. As mentioned in Section 3.2.1, the luminescence emission centered at 440 nm is likely related to Bi^{3+} which has a nanosecond lifetime with matrix emission in the background.

The luminescence emission from the matrix, Fig. 7a, centered at 650 nm appears to be significantly suppressed at a Bi_2O_3 concentration of 0.5 mol%. The associated excitation spectra in Fig. 7d, indicate a similar trend with the longer wavelength peak whose leading edge is excited into at 325 nm gradually shifting from being centered at 348 nm (undoped) to 384 nm (1 mol% Bi_2O_3 doped) with the shift largely accomplished by the 0.5 mol% Bi_2O_3 doping level.

Finally, the excitation bands centered at 450–460 nm associated with the emission at 810 nm, Fig. 7e, are fully shifted from those characteristic of an undoped sample to those associated with a sample doped with Bi_2O_3 by a concentration level of 0.01 mol%. The very weak excitation bands at 325 nm are the reason for the absence of this emission, however, the excitation band in the 400–500 nm spectral region where the emission at 810 nm is the strongest is approximately 60 times greater than what it is at 325 nm for the 1 mol% Bi_2O_3 doping case. To conclude, the evolution of the broadband emission as well as the emissions centered at 450 and 815 nm are indicative of a complex process associated with evolution of the glass structure as the concentration of Bi_2O_3 is increased.

4. Conclusions

The role of the germanate glass matrix and the bismuth dopant concentration on emission behavior within the visible and near infrared spectral regions has been investigated and correlated to the matrix-environment defect level and dopant valence states. A significant shift in the luminescence spectra (out to 900 nm) between NBO high/low and NBO zero/zero- undoped and bismuth doped glasses was seen to occur and attributed to (1) differing defects which form in the two classes of glass matrices (NBO high/low *vs.* NBO zero/zero-) resulting in the formation/stabilization of different sorts of bismuth emission centers having unique emission as well as (2) the tightening of the glass structure as the Na/Al ratio decreased resulting in increased crystal field splitting with an accompanying shift of emission to shorter wavelengths. Bismuth specific emissions were characterized and tentatively identified at 450 nm (likely Bi^{3+} emission), 615 nm (likely Bi^{2+}) and 810 nm (possibly Bi^{0}) from the NBO high/low matrices and at 775 nm (possibly Bi^{2+}) from NBO zero/zero- glasses. With the addition of bismuth to a (1) NBO low matrix excited with 248 nm, elimination of the absorption associated with emission from the matrix in the 420 nm region (GLPC region) coincided with the emergence of dominant Bi^{2+} emission centered at 615 nm, and (2) NBO high glass excited with 325 nm, the elimination of the broadband matrix emission centered at ~650 nm coincided with the simultaneous growing in of a bismuth related emission, likely Bi^{3+}, centered at 440 nm. Additional work is needed to fully understand the complex processes which occur when multivalent bismuth is added to a soda alumino germanate glass matrix. Finally, investigation of the emission properties of identical bismuth doped glasses in the 900–1600 nm spectral range for longer excitation wavelengths will be presented in a future publication.

Author contributions

Conceptualization: L. J. Henry conceived idea in conjunction with K. A. Richardson, M. L. Klopfer and L. J. Henry collected the data, L. J. Henry and J. Reding analyzed the data, L. J. Henry wrote the manuscript and J. Reding and K. A. Richardson reviewed the manuscript.

Conflicts of interest

The views expressed are those of the authors and do not necessarily reflect the official policy or position of the Department of the Air Force, the Department of Defense, or the US Government.

Data availability

Additional data supporting this article has been included as part of the supplementary information (SI). Supplementary information is available. See DOI: **https://doi.org/10.1039/d5tc02646f**.

Acknowledgements

L. J. Henry would like to acknowledge the Air Force Research Laboratory for their support throughout this work.

References

1 B. Mukherjee, *IEEE J. Sel. Areas Commun.*, 2000, **18**, 1810–1824.
2 R. Essiambre, G. Kramer, P. J. Winzer, G. J. Foschini and B. Goebel, *J. Light Technol.*, 2010, **28**, 662–701.
3 S. Tanabe, *C. R. Chim*, 2002, **5**, 815–824.
4 G. Keiser, *Optical Fiber Communications*, 3rd edn, The McGraw-Hill Companies, New York, 2000.
5 G. A. Thomas, B. I. Shraiman, P. F. Glodis and M. J. Stephen, *Nature*, 2000, **404**, 262–264.
6 N. K. Thipparapu, Y. Wang, S. Wang, A. A. Umnikov, P. Barua and J. K. Sahu, *Opt. Mater. Express*, 2019, **9**, 2446–2465.
7 K. Murata, Y. Fujimoto, T. Kanabe, H. Fujita and M. Nakatsuka, *Fusion Eng. Des.*, 1999, **44**, 437–439.
8 Y. Fujimoto and M. Nakatsuka, *Jpn. J. Appl. Phys.*, 2001, **40**, L279–L281.

9 S. V. Firstov, S. V. Alyshev, K. E. Riumkin, A. J. Khegai, A. V. Kharakhordin, M. A. Melkumov and E. M. Dianov, *IEEE J. Sel. Top. Quantum Electron.*, 2018, **24**, 0902415.
10 N. K. Thipparapu, Y. Wang, A. A. Umnikov, P. Barua, D. J. Richardson and J. K. Sahu, *Opt. Lett.*, 2019, **44**, 2248–2251.
11 A. Donodin, E. Manuylovich, V. Dvoyrin, M. Melkumov, V. Mashinsky and S. Turitsyn, *APL Photonics*, 2024, **9** 046102.
12 S. Khonthon, S. Morimoto, Y. Arai and Y. Ohishi, *Opt. Mater.*, 2009, **31**, 1262–1268.
13 J. A. Duffy and M. D. Ingram, *J. Non-Cryst. Solids*, 1976, **21**, 373–410.
14 B. Xu, S. Zhou, D. Tan, Z. Hong, J. Hao and J. Qiu, *J. Appl. Phys.*, 2013, **113**, 083503.
15 A. S. Zlenko, V. M. Mashinsky, L. D. Iskhakova, R. P. Ermakov, S. L. Semjonov and V. V. Koltashev, *Quantum Electron.*, 2013, **43**, 656–665.
16 M. Y. Sharonov, A. B. Bykov and R. R. Alfano, *J. Opt. Soc. Am. B*, 2009, **26**, 1435–1441.
17 T. Izumitani, B. Peng and K. Richardson, *Rev. Laser Eng.*, 1996, **24**, 59–64.
18 K. Cerqua-Richardson, B. Peng and T. Izumitani, *Proc. Adv. Solid-State Lasers*, 1992, **13**, 52–55.
19 G. Blasse and A. Bril, *J. Chem. Phys.*, 1968, **48**, 217–222.
20 D. Van Der Voort and G. Blasse, *J. Solid State Chem.*, 1992, **99**, 404–408.
21 S. Lai, Z. Yang, R. Wang, H. Wu, J. Liao, J. Qiu, Z. Song, Y. Yang and D. Zhou, *J. Mater. Sci.*, 2013, **48**, 8566–8570.
22 Y. Zorenko, M. Pashkovsky, A. Voloshinovskii, B. Kuklinski and M. Grinberg, *J. Lumin.*, 2006, **116**, 43–51.
23 A. Novoselov, A. Yoshikawa, M. Nikl, J. Pejchal and T. Fukuda, *J. Cryst. Grow.*, 2006, **292**, 236–238.
24 G. Blasse, A. Meijerink, M. Nomes and J. Zuidema, *J. Phys. Chem. Solids*, 1994, **55**, 171–174.
25 M. Gaft, R. Reisfeld, G. Panczer, G. Boulon, T. Saraidarov and S. Erlish, *Opt. Mater.*, 2001, **16**, 279–290.
26 M. A. Hamstra, H. F. Folkerts and G. Blasse, *J. Mater. Chem.*, 1994, **4**, 1349–1350.
27 X. Wang, S. Xu, Z. Yang and M. Peng, *Opt. Lett.*, 2019, **44**, 4821–4824.
28 A. M. Srivastava, *J. Lumin.*, 1998, **78**, 239–243.
29 J. Zheng, L. Tan, L. Wang, M. Peng and S. Xu, *Opt. Express*, 2016, **24**, 2830–2835.
30 A. N. Romanov, A. A. Veber, Z. T. Fattakhova, O. V. Usovich, E. V. Haula, L. A. Trusov, P. E. Kazin, V. N. Korchak, V. B. Tsvetkov and V. B. Sulimov, *J. Lumin.*, 2013, **134**, 180–183.
31 A. G. Okhrimchuk, L. N. Butvina, E. M. Dianov, N. V. Lichkova, V. N. Zagorodnev and K. N. Boldyrev, *Opt. Lett.*, 2008, **33**, 2182–2184.
32 L. Su, H. Zhao, H. Li, L. Zheng, G. Ren, J. Xu, W. Ryba-Romanowski, R. Lisiecki and P. Solarz, *Opt. Lett.*, 2011, **36**, 4551–4553.
33 J. Zheng, M. Peng, F. Kang, R. Cao, Z. Ma, G. Dong, J. Qiu and S. Xu, *Opt. Express*, 2012, **20**, 22569–22578.
34 X. Jiang and A. Jha, *Opt. Mater.*, 2010, **33**, 14–18.
35 Z. Zhang, J. Cao, J. Zheng, M. Peng, S. Xu and Z. Yang, *Chin. Opt. Lett.*, 2017, **15**, 121601.
36 L.-S. Du and J. F. Stebbins, *J. Phys. Chem. B*, 2006, **110**, 12427–12437.
37 M. Y. Peng, J. R. Qiu, D. P. Chen, X. Meng, I. Yang, X. Jiang and C. Zhu, *Opt. Lett.*, 2004, **29**, 1998–2000.
38 H. Luo, J. Cao, X. Li, X. Wang and M. Peng, *J. Mater. Chem. C*, 2018, **6**, 11525–11535.
39 E. J. Friebele, D. L. Griscom and G. H. Sigel Jr, *J. Appl. Phys.*, 1974, **45**, 3424–3428.
40 A. K. Varshneya and J. Mauro, *Fundamentals of Inorganic Glasses*, 3rd edn, Elsevier, Cambridge, Massachusetts, 2019.
41 K. Kamiya and S. Sakka, *Phys. Chem. Glasses*, 1979, **20**, 60–64.
42 L. Wang, L. Tan, Y. Yue, M. Peng and J. Qiu, *J. Am. Ceram. Soc.*, 2016, **99**, 2071–2076.
43 L. L. Tan, A. Qiao, C. G. Lin, Y. Yue and M. Peng, *J. Alloys Compd.*, 2022, **898**, 162884.
44 W. Chen, X. Huang, Q. Dong, P. Xiong, D. Yang, J. Qiu, Z. Yang and G. Dong, *J. Mater. Chem. C*, 2024, **12**, 459–467.
45 L. N. Skuja, *Phys. Status Solidi A*, 1989, **114**, 731–737.
46 L. Skuja, H. Hosono, M. Mizuguchi, G. Güttler and A. Silin, *J. Lumin.*, 2000, **87–89**, 699–701.
47 M. Hongisto, A. Veber, Y. Petit, T. Cardinal, S. Danto, V. Jubera and L. Petit, *Materials*, 2020, **13**, 3846.
48 H. Kawazoe, *J. Non-Cryst. Solids*, 1985, **71**, 231–243.
49 G. Kordas, R. A. Weeks and D. L. Kinser, *J. Appl. Phys.*, 1983, **54**, 5394–5399.
50 T. Asahi, Y. Omura, N. Wada and S. Nakayama, *Optik*, 2017, **149**, 423–429.
51 J. Ueda, A. Hashimoto and S. Tanabe, *J. Phys. Chem. C*, 2019, **123**, 29946–29953.
52 E. M. Dianov, *Quantum Electron.*, 2010, **40**, 283–285.
53 E. M. Dianov, *Laser Phys. Lett.*, 2015, **12**, 095106.
54 L. J. Henry, C. Hefner and M. L. Klopfer, submitted.
55 N. Zhang, J. Qiu, G. Dong, Z. Yang, Q. Zhang and M. Peng, *J. Mater. Chem.*, 2012, **22**, 3154–3159.
56 R. J. Ginther and R. D. Kirk, *J. Non-Cryst. Solids*, 1971, **6**, 89–100.
57 E. M. Dianov, *Light: Sci. Appl.*, 2012, **1**, e12.
58 I. Razdobreev, H. El Hamzaoui, V. Y. Ivanov, E. F. Kustov, B. Capoen and M. Bouazaoui, *Opt. Lett.*, 2010, **35**, 1341–1343.
59 A. A. Veber, O. V. Usovih, L. A. Trusov, P. E. Kazin and V. B. Tsvetkov, *Luminescence centers in silicate and germanate glasses activated by bismuth*, Bulletin of the Lebedev Physics Institute, 2012, vol. 39, pp. 305–310.

